Hybrid Microassembly Combining Robotics and Water Droplet Self-Alignment

Veikko Sariola, Mirva Jääskeläinen, and Quan Zhou, *Member, IEEE*

***Abstract*—This paper reports an in-depth study of a hybrid microassembly technique that combines a robotic micromanipulator and a water droplet self-alignment, which greatly improves the performance of robotic microassembly. The method is experimentally studied on a custom-made microrobotic test platform adapted for the experiments. Four important measures of the microassembly technique are investigated—yield, capability, accuracy, and speed. Yield is studied by a large number of tests with random process parameters and statistical-modeling methods. Accuracy is measured by studying the final assembly results under a scanning electron microscope (SEM). Capability is assessed by testing parts of various sizes and shapes. Using a high-speed camera, the duration and trajectories of droplet self-alignment of the hybrid assembly process are studied. The experimental results indicate that such a hybrid assembly technique has very low requirements on the precision, which is comparable with the dimensions of the micropart, of the handling robot while being able to achieve micrometer precision. Moreover, successful assembly can be easily achieved with part sizes that range from 50 to 300 μm. The experiments also show that parts of different sizes can be reliably assembled together using the proposed method.**

***Index Terms*—Droplet self-alignment, hybrid microassembly, microassembly, micro-/nanorobots, self-assembly.**

I. Introduction

While the miniaturization of microelectronics and systems still continues, the current trend is toward more intelligent and multifunctional devices [1]. Dubbed as "More than Moore" [2], this requires integrating different types of components, such as logic, memory, radio frequency, signal conditioning, sensors, actuators, mechanics, fluidics, optoelectronics, and optics, into a single device. Even though specific manufacturing processes exist for each type of component, the processes are often hard or impossible to combine into a monolithic manufacturing process. The solution is to manufacture the components separately and integrate them using an advanced microassembly technology.

A typical microassembly procedure includes the following major steps: feeding, positioning, bonding, making electrical connections, and packaging. In some cases, two or more of these can be combined into one step, as in flip chip, in which the bumps serve both as mechanical fixing and electrical connection. Until recently, high-speed robotics has been able to achieve the required accuracy, reliability, capability, and throughput needed in positioning. However, the current trends in microsystem technology, such as the miniaturization of dies, the smaller pad pitch because of the increased number of input/output, 3-D structures, the adaption of system-in-a-package, and through-silicon-via technologies, are pushing the limits of robotics. Therefore, new solutions to position microparts are required.

A. Hybrid Microassembly

The approaches to assemble micro- and nanosystems can be broadly categorized into two branches: robotic assembly and self-assembly. The former uses robotic tools, e.g., microgrippers, to pick-and-place parts to the desired position. In the latter, the part positioning and alignment occur spontaneously because of the parts being attracted to energy minimum.

Robotic microassembly has been actively researched since the early 1990s [3]–[9]. A typical robotic microassembly station is composed of one or more tools (e.g., a mechanical gripper or a vacuum microgripper), several motion stages, a vision system, and illumination. Initially, the assembly stations were teleoperated [3], but the trend is toward increased automation and intelligence [4]–[9].

Self-assembly in chemistry and biology has been discussed for several decades [10], [11]. Since the early 1990s, the concept has been extended to the assembly of microscopic parts [12]–[18]. Self-assembly of microparts is typically based on surface interactions. Often, the procedure is performed in liquid with a large number of microparts and receptor sites. The microparts are attracted randomly to the receptor sites through the so-called principle of minimum potential energy, where the system will seek to an energy minimum by dissipating energy, e.g., as heat. To avoid being trapped in a local minimum, a perturbation signal (e.g., vibrations or fluid flow) is often applied to overcome the energy barriers.

Both robotic microhandling and self-assembly have their strengths and weaknesses. Robotic microhandling can perform rather complex tasks through dexterous manipulation and advanced end-effectors. In low-cost, mass-manufacturing

Manuscript received March 3, 2010; revised August 6, 2010; accepted August 6, 2010. Date of publication September 13, 2010; date of current version December 8, 2010. This paper was recommended for publication by Associate Editor M. Sitti and Editor K. Lynch upon evaluation of the reviewers' comments. This work was supported in part by the European Commission under Grant NMP2-CT-2006-026622 Hybrid Ultra Precision Manufacturing Process Based on Positional- and Self-Assembly for Complex Micro-Products, HYDROMEL (2006–2010), in part by the Academy of Finland under Grant 134206 Programmable and Spatially Multi-Scale Self-Assembly of Microcomponents, MUSA (2010–2013), and in part by the Graduate School in Electronics, Telecommunication, and Automation. An earlier version of this work was presented at the IEEE/RSJ International Conference on Intelligent Robots and Systems, Nice, France, 2008.

The authors are with the Department of Automation and Systems Technology, School of Science and Technology, Aalto University, 00076 Aalto, Finland (e-mail: veikko.sariola@tkk.fi; mirva.jaaskelainen@gmail.com; quan.zhou@tkk.fi).

Color versions of one or more of the figures in this paper are available online at http://ieeexplore.ieee.org.

Digital Object Identifier 10.1109/TRO.2010.2066830

applications, around 100 000 parts/h [19] throughput is achievable at a relatively low accuracy of tens of micrometer. If high accuracy is needed, the throughput has to be dramatically lowered. In contrast, self-assembly often has a relatively high throughput (up to 2 million parts/h [20]) and high accuracy because of the nature of parallel process. However, the parallel, batch nature of self-assembly process requires the whole template be specially designed for self-assembly and have no local minima, which limits the applicability of self-assembly.

The border of these two branches is not so clear. If we analyze the development of robotic microhandling during the past few years, we can see that the principle of minimum potential energy is also used in various situations, such as in self-centering of capillary gripper [21], in snap locking [8], and in optical tweezers [22]. Moreover, perturbation is also used in the vibration release of micropart [23]. On the other hand, the common approach of coarse-fine positioning of robotic microhandling can also be found in self-assembly [24]. In our previous publications [25], [26], we analyzed similarities of the both by finding common technical elements, such as process steps, ambient environment effects, and surface and material effects on the assembly processes.

Because of the similarities, a promising approach to design a microassembly technique is to consider each of the elements without considering if the approach should be robotic or self-assembly in nature by combining the two approaches into so-called hybrid microassembly or hybrid microhandling technique. There are many ways to create these hybrid techniques. For example, robotics can be used to correct the errors of a stochastic self-assembly process, whereas self-alignment can be used for the final positioning after robotic microassembly.

In a previous study of Zhou and Chang [27], the concept and potential merits of this hybrid microhandling are evaluated, but no extensive experimental studies have been carried out.

B. Droplet Self-Alignment

When a droplet of liquid is constrained between two surfaces of matching shape, a meniscus forms between the surfaces and the surface tension of liquid will align the surfaces to each other. This can be used to align microparts to receptor sites. For example, the effect can be found in flip-chip soldering [28], [29]. The constraining of the liquid can be achieved by the wetting properties of the surfaces [28]–[30]. For example, 1 mm $\times$ 1 mm parts with hydrophilic/phobic patterns have been used for water droplet self-alignment [30]; however, the alignment accuracy was still relatively low, and reliability was not proven. The constraining can also be achieved by using a solid edge [31], [32]. In the work of Tsai *et al.* [31], 1 mm $\times$ 1 mm radio-frequency identification chips were aligned using water droplets. However, the effects of process parameters on the self-alignment were not thoroughly examined. Earlier, the authors studied the accuracy of droplet self-alignment of microparts of the size 300 μm $\times$ 300 μm $\times$ 70 μm as a function of the part location and the amount of liquid [32].

Droplet self-alignment is commonly used in fluidic self-assembly [15], [16], [18] or in dry self-assembly [24]. In a typical setup, the receptor sites are covered with adhesive, which "wets" the microparts upon contact and aligns and bonds them to the receptor sites.

Oscillations of a self-aligning circular pad (3.8 mm in diameter) on a droplet have also been studied [33], where a circular pad was placed on a droplet and carefully perturbed using a needle. The pad oscillated shortly before settling into equilibrium, and the oscillations were recorded using a high-speed camera. Whereas the work in [33] is valuable development toward understanding the dynamics of droplet–part interaction, it is difficult to extrapolate the dynamics (e.g., trajectories) of the actual assembly sequence based on those results.

Capillary forces in droplet self-alignment have been extensively modeled using analytical and numerical tools, e.g., see [34], [35]. However, to predict yield, accuracy, trajectories, or statistical variations in droplet self-alignment duration is very difficult using these tools. These parameters are very interesting for practical applications of the hybrid handling method.

C. Objective

The objective of this study is to systematically evaluate the potential of a hybrid microassembly approach that uses a robot for coarse positioning and droplet self-alignment for fine positioning. The aim is to justify if this method can be used for high-throughput, high-precision, and high-yield microassembly. In this study, we use small, cuboid-shaped parts, which range from 50 μm $\times$ 50 μm $\times$ 40 μm to 300 μm $\times$ 300 μm $\times$ 70 μm, which are close to the limits of robotic-microhandling technology. To assess the benefits of this positioning technique, we experimentally evaluate four performance measures–accuracy, speed, yield, and capability–of the process.

This proposed approach is very different from other droplet self-alignment work, where those studies are on droplet self-alignment processes, and this paper studies the hybrid microassembly process as an automation strategy, which includes also the robot. For this purpose, this study explores very thoroughly the process parameters that have never been studied in this level of detail. This thorough study is extremely important for future process design and scaling hybrid microassembly into real-world applications.

Compared with solder self-alignment in flip-chip applications, the method is very different, as the water droplet wets not only the single pad but the whole surface of the chip as well. The self-alignment is able to correct errors comparable with the chip size when solder self-alignment is able to correct only errors comparable with pad size. Moreover, the capillary forces of the water droplet help to overcome one of the major problems in microassembly: the adhesion between the tool and the part. This does not happen if the solder reflow is done only afterward in an oven.

Another difference of this method to most self-alignment or self-assembly method is that no patterning of the parts is needed. Only the solid edge of the micropart is used to constrain the liquid. This further allows stacking multiple dies with similar top and bottom surfaces on top of each other.

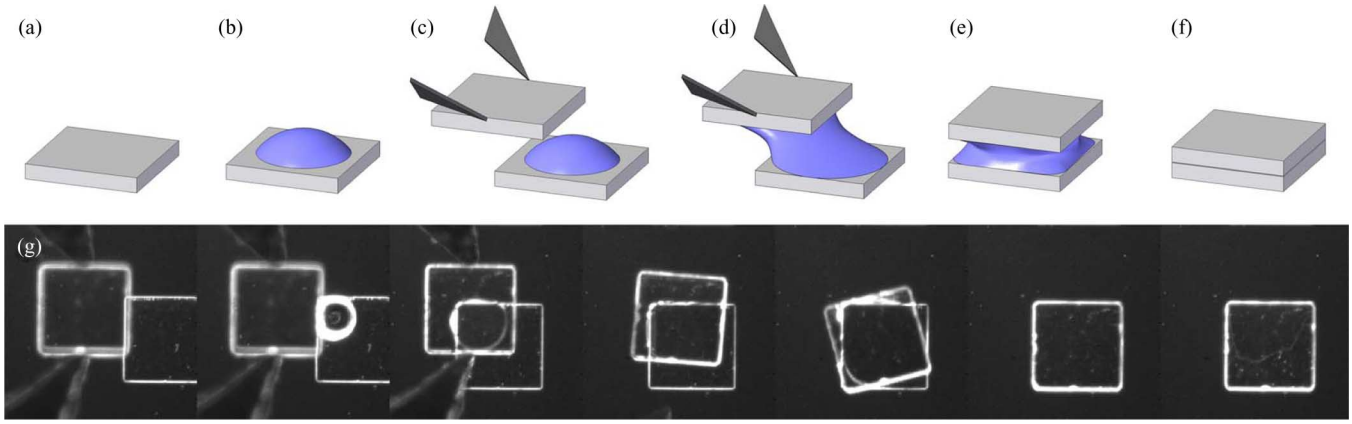

Fig. 1. Hybrid handling technique. (a) Assembly site is on top of a micropart. (b) Droplet of water is dispensed on the bottom part. (c) Microgripper approaches the release site with a part. (d) Droplet contacts with the top part and wets between the parts, which forms a meniscus. (e) Microgripper releases the part and the capillary force aligns the parts. (f) Water between the two parts evaporates, which leaves the two parts aligned. (g) Image sequence of the actual experiment, as viewed from the top side.

The parts are also significantly smaller than those used in most of previous work, e.g., 1 mm $\times$ 1 mm in [30] and [31]. Furthermore, to the knowledge of the authors, no studies have been performed using parts that do not match the shape of the receptor site, which need not be the case, as discussed in Section II-D and experimentally shown in Section V.

In the next section, the experimental methods are detailed. In Section III, the apparatus is introduced. In Section IV, the yield of the process and statistical modeling methods used for yield are presented. Section V contains experimental results on the capability, accuracy, and speed of the process. Section VI contains discussion of the results. Section VII concludes the paper.

An earlier stage of this study was presented in the *IEEE/RSJ International Conference on Intelligent Robots and Systems* [36]. In Section IV, three completely new test sets have been conducted in addition to the original one test set, and completely new statistical analysis is included. This significantly expands the depth of the study. Section V-B has never been reported. Sections II–IV, V-A, and V-C have been extended with new insight and in-depth analysis of the process.

II. Methods

This section outlines the elements of the proposed hybrid-microassembly process, including the selection of tools, different liquids that can be used, and different parameters that affect the hybrid assembly process.

A. Basic Procedure

The basic handling sequence is illustrated in Fig. 1. The robotic microgripper first picks a micropart from a reservoir of microparts and carries it near the receptor site, which is actually another part fixed to a substrate. Then, the dispenser dispenses a droplet of water on the receptor site. The robot then carries the part over the receptor site so that the droplet wets the surfaces of both parts, and a meniscus is formed. After this, the microgripper quickly opens, which releases the part from its grasp. The surface tension of the droplet then aligns the part to the receptor site. Finally, the droplet evaporates and leaves the part aligned with the receptor site. In Fig. 1, the part and the receptor site have exactly the same size and shape, but as discussed in Section II-D, this need not be always the case.

B. Selection of Tools

In this study, a tweezer-type microgripper [37] is used. Picking microparts in this size range is usually easy; however, the release is severely hindered by adhesion forces. The smallest microparts can easily be picked up with one tip of the gripper by using adhesion forces only.

The reason a tweezer-type microgripper was chosen instead, e.g., a vacuum gripper [30], is that the microgripper allows the micropart to be viewed from the top side, which helps to image the process. Another approach to achieve similar view would be using a transparent surface and having the microscope mounted below the surface. However, that would require fully transparent part carrier and more complicated illumination and motion systems.

A noncontact dispenser is used to dispense droplets at the receptor sites. As long as the water is dispensed on top of a receptor site, a meniscus may form between the part and the receptor site. The capillary force of the meniscus overcomes the tool-part adhesion, and consequently, the micropart aligns with the receptor site.

C. Liquid Medium and Bonding

The self-alignment has been studied using various liquids, including water [30] and ethylene glycol [32]. The reason ethylene glycol was used in some tests is that it resembles certain UV-curable adhesive in viscosity. With UV-curable adhesive, the final bonding of the part could be done by simply applying UV-light.

In this study, water is used. Water evaporates rather quickly, which allows multiple tests using the same parts in a reasonably short timescale. In our experience, the part will be weakly

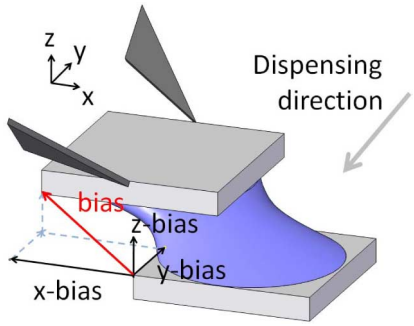

Fig. 2. Definition of bias. The bias is defined as the difference between the release position and the final position of the assembled micropart after successful self-alignment.

bonded by adhesion after the water is evaporated. This bonding is still much stronger than gravity: Often, it is even difficult to detach the microparts with our gripper after the water has evaporated. If a stronger bonding is needed, it can be achieved afterward, e.g., by coating the whole structure with adhesive or by thermal bonding.

An application of the water-based assembly would be aligning chips on an alignment template with bumped side up before performing wafer-level flip-chip bonding. Another application is to perform droplet self-alignment with bumped side down, which is followed by solder reflow of the bumps.

D. Bias

The position difference between the release position and the final position is defined as *the bias*, as shown in Fig. 2. In most of the tests, the effect of the bias to the self-alignment process is studied, as it has been previously reported that the result of the assembly can depend on it [30]. When the shape of the micropart and the receptor site are not perfectly matching, the bias is especially important. If, e.g., a square-shaped part will be placed on top of a bar-shaped receptor site, theoretically, the location of the square-shaped part is ambiguous [27], as shown in Fig. 3(a). However, when the initial bias is outside one end of the bar, the part will deterministically align to that end, as shown in Fig. 3(b).

E. Target of Droplet Dispensing

One important consideration is where the water should be dispensed. In Fig. 4, two locations can be identified: the release position so that the droplet is below the middle point of the part when releasing and the expected final position so that the droplet is over the middle point of the receptor site. This has subtle, but large implications: When dispensing the water into the final location, the water is guaranteed to be on top of the receptor site. However, when dispensing to the release location, the water may be close to the boundary of the receptor site so that it easily spills and does not stay on top of it. Furthermore, if the release location is outside the receptor site, there is no chance for water to stay on top of the receptor site to form the necessary meniscus for self-alignment.

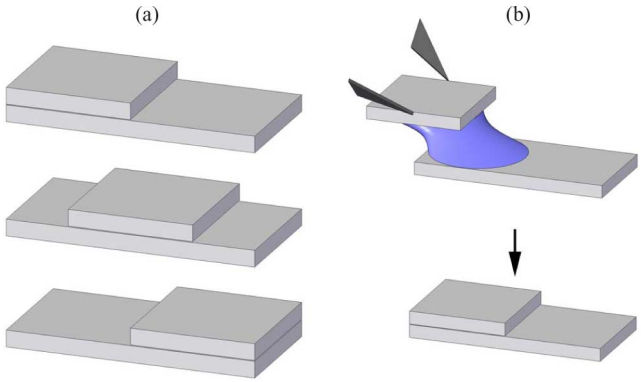

Fig. 3. (a) Ambiguous final positioning of part and receptor site with different sizes if the self-alignment succeeds. (b) Starting the hybrid microhandling with the part outside the receptor site, the part is deterministically aligned to the side of the receptor site.

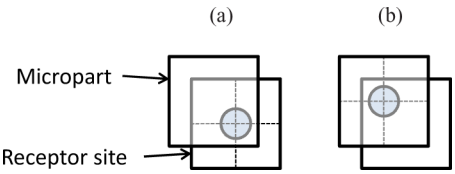

Fig. 4. Water can be dispensed either at the (a) final location, which is in the middle of the receptor site, or at the (b) release location.

Whichever dispensing location is more realistic depends on the assembly task: whether the dispenser is fixed in the reference frame of the release site or the reference frame of the gripper. Of these two options, fixing of the dispenser in the reference frame of the gripper can be expected to be more common, as it is often easiest in robotic microhandling to move the parts and keep gripper, dispenser, and microscopes fixed. In such a setup, it is more realistic to dispense the water at the releasing position.

F. Alignment of the Parts

Before the tests, the part is manually aligned to the receptor site. When doing series of tests, if a test is successful, the part can be assumed to be aligned to the receptor site with an accuracy of about 2 μm, as shown in Section V-B. The part can then be directly picked for the next experiment, as this error is much smaller than the biases used in the experiments. Assuming successful picking, the orientation (roll-pitch-yaw) of the part before releasing is the same as the orientation of the receptor site. However, small errors in orientation are always present because of the randomness of the adhesion of the part to the substrate during picking and the imperfections of the gripper tips. Since the errors are small and hybrid handling is capable of correcting even big angular errors [27], the orientation difference can be neglected.

III. Apparatus

The complete test system is shown in Fig. 5. The figure also includes the coordinate axes used throughout the text.

The microgripper is custom-designed and uses two piezoelectric bender actuators to open and close the gripper [37]. The

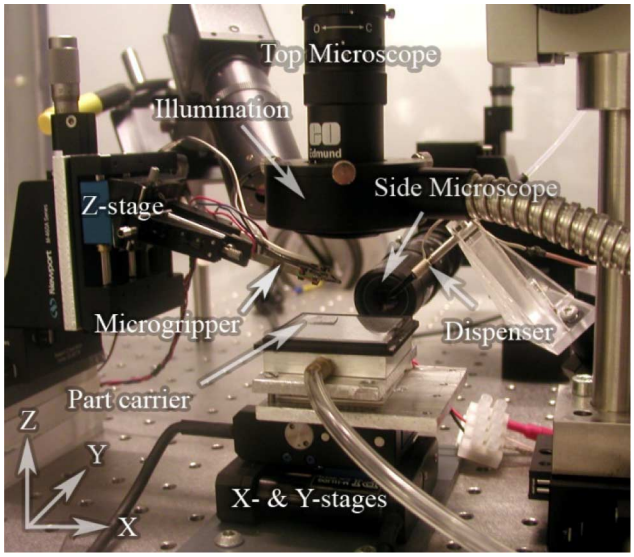

Fig. 5. Overview of the apparatus.

actuators are driven in open loop. Both benders have a maximum displacement of ± 250 μm so that the gripper has an opening of 1 mm. Tips made from stainless steel have been used. Three translational stages (manufacturer/model: PI/M111.1DG) are used to generate translational motion in the system. Each stage has a travel range of 15 mm and a unidirectional repeatability of 100 nm. The Z-stage can be used to move the microgripper up and down, while the X- and Y-stage can be used to move the part carrier. The part carrier is mounted on the X- and Y-stage. A part carrier is a polished silicon die, which is the same as the one on which the parts were originally fabricated. The microparts are fabricated from SU-8, which is spincoated, exposed, developed, and hard baked on top of a thin layer of aluminum. As the adherence of SU-8 to aluminum is not very strong, the smallest parts can be detached from the wafer just by applying force. For the larger parts, the aluminum can be partially etched away to help the release. The fabrication process is better described in [38].

The dispenser is a noncontact dispenser (manufacturer/model: Gesim/PicPIP), which is actuated by a piezoelectric diaphragm. The bending of the diaphragm leads to compression of liquid inside a chamber and ejection of a droplet from a nozzle. The volume of each droplet can be tuned between 100 and 400 pL, which depends on the dispenser parameters, i.e., the pulsewidth and amplitude of the actuation signal. By dispensing multiple droplets, a larger droplet can be formed. Fine tuning the size of the droplet can be achieved by letting the water evaporate before starting the self-alignment.

The handling process is imaged from the top with a microscope (manufacturer/model: Edmund/VZM1000i) with an adjustable optical zoom between 2.5 $\times$ –10$\times$. The top microscope has a high-speed charge-coupled device (CCD) camera (manufacturer/model: Imperx/IPX-VGA210-G). By using the maximum possible frame size of 640 $\times$ 480 pixels, a framerate of about 210 frames/s is achieved. However, by using smaller area of interest (AOI), higher framerates (up to 3000 frames/s) can be achieved. Most of the tests are not recorded with full frame size but with smaller AOI. As long as the corners of both the micropart and the receptor site are shown in the picture, their relative positions and orientation can be estimated.

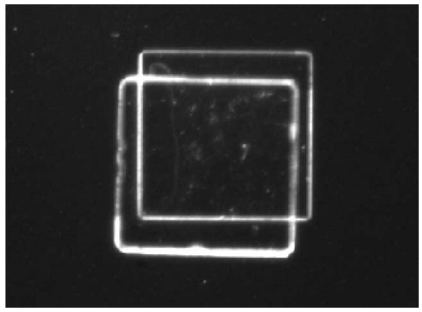

Fig. 6. Results of a failed hybrid assembly experiment.

The top microscope is integrated with halogen fiber-optic ring illumination. This avoids heating of the system, which can speed up the evaporation of the droplets. Furthermore, the system includes another two microscopes: one to image from the side and other to give an overview of the process to the operator. Normal video framerate CCD cameras are used in these two systems.

IV. Yield

To assess the assembly technique, we first measure the yield of process. Yield is the proportion of successful assemblies out of all tests in a specific test set, as a function of bias and droplet volume. This is studied by a large number of tests with random process parameters. The results are then analyzed using logistic regression.

Based on our initial experiences with the handling method, it is largely a binary process: It either succeeds or fails completely. Successful hybrid handling is defined as a part self-aligning and the accuracy not being distinguishable from the image of the optical microscope. Failure is defined as the part that gets stuck in a local minimum, typically almost 50 μm away from the correct position, and then, the water evaporates, which leaves the part misaligned (see Fig. 6). Sometimes, the self-alignment never starts, because the bias is so large that no meniscus forms between the part and the receptor site.

A. Preliminary Tests: Dispensing Water on Receptor Sites

Before the actual handling tests, the maximum allowable x and y biases were checked by dispensing water on the parts. The dispensing was considered successful when major part of the droplet stays on top of the receptor site.

The successful dispensing area was determined by dispensing 200 times 0.7 nL droplets on the top of a 300 μm $\times$ 300 μm part and 0.2 nL droplet on the top of a 100 μm $\times$ 100 μm part with a varying bias. The test area was 600 μm $\times$ 600 μm in the former and 200 μm $\times$ 200 μm in the latter.

The results are shown in Fig. 7. The area is quite rectangular and very close to the size of the part. Therefore, it is concluded that there are no accidental spilling of water as long as the

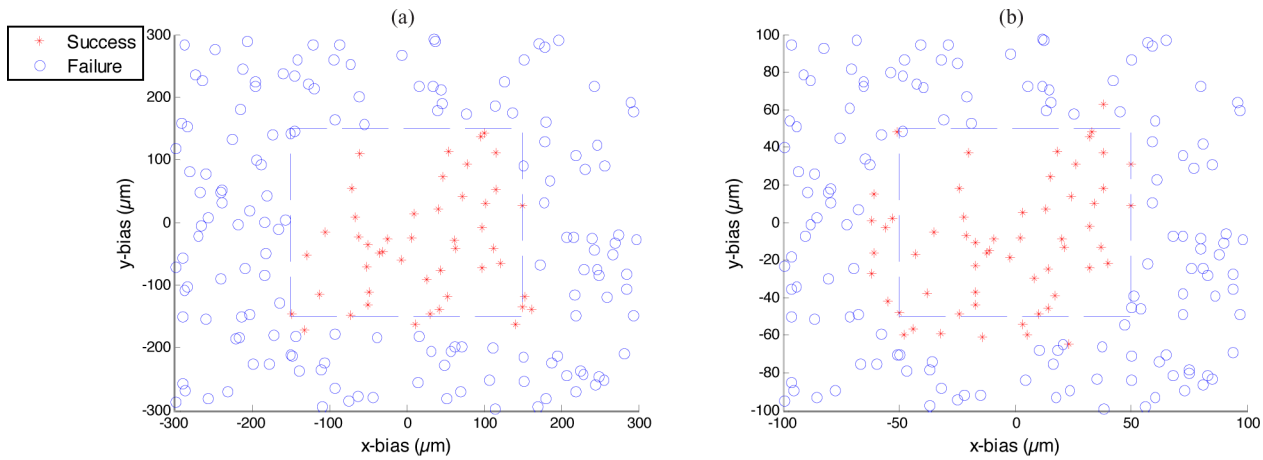

Fig. 7. Results of the droplet-dispensing test. Success of dispensing on top of (a) the 300 μm $\times$ 300 μm part and (b) the 100 μm $\times$ 100 μm part. Dashed line indicates the location of the receptor site.

TABLE I
PARAMETERS OF YIELD TEST SETS

Parameter	Test set 1	Test set 2	Test set 3
Part size (μm)	300 × 300	300 × 300	100 × 100
X- & Y-bias (μm)	-250 … 250	-250 … 250	-100 … 75
Z-bias (μm)	0 … 50	0 … 75	0 … 50
Liquid (nl)	0.3 … 2.7	0.2 … 3.2	0.2 … 0.7
Water location	Final location	Release location	Release location
Number of tests	192	352	240

droplet is dispensed inside the boundaries of the receptor site. In Fig. 7(b), the successful dispensing area does not exactly match the shape of the receptor site and is not exactly symmetric because of the tilt of the dispenser.

B. Assembly Tests

Three different test sets were conducted by varying four different parameters, i.e., x-y-z-bias and the amount of liquid, randomly. The parameters of the test sets are shown in Table I. The parameters were chosen based on our initial explorative study. Any parameters outside these boundaries seemed unlikely to be successful.

In the test set 1, the droplet is dispensed at the center of the receptor site and in test sets 2 and 3, the droplet is dispensed in the release position. The impact of these choices was discussed in Section II-E.

Test set 3 studied the assembly of smaller parts. The part size was dropped to 100 μm $\times$ 100 μm, and other parameters were adjusted accordingly (smaller biases and smaller amount of water).

The results of the test sets are illustrated in Fig. 8. Test set 2 is further illustrated in Fig. 9. The success rates were 69%, 48%, and 38% for each test set, respectively.

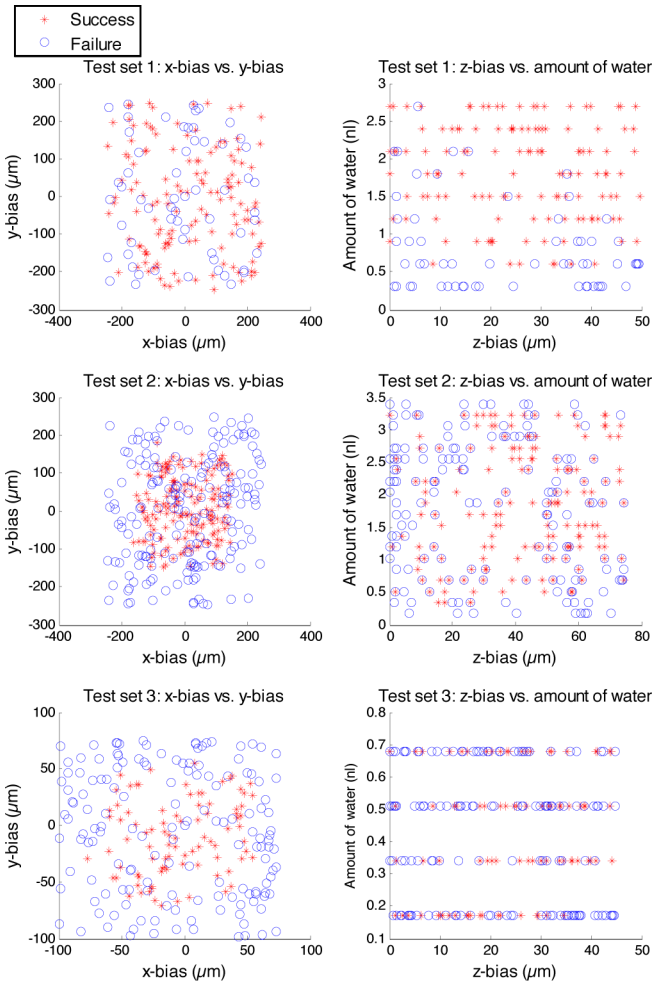

Fig. 8. Results of the three different test sets.

C. Statistical Modeling

Because of the stastistical nature of the process, regression model is used to filter out noise and extract most important parameters of the process.

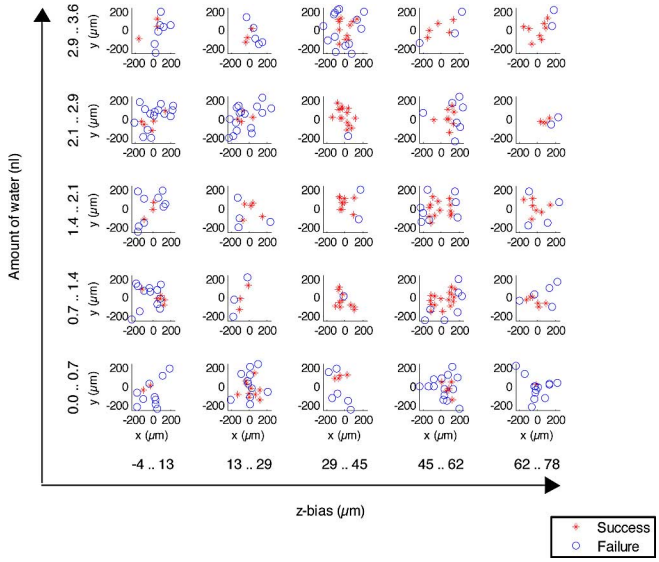

Fig. 9. Breakdown of the error tests in test set 2. Each subplot shows a range of z-bias and amount of water. Inside each subplot, it can be seen that the successes are mostly concentrated in the middle. The failures with large x-bias and y-bias are due to failed dispensing.

We have four process parameters: x, y, z, V, which represent bias in x, y, and z axes (unit in micrometer) and the volume of liquid (unit in nanoliter), respectively. Each test has a binary outcome $S \in \{0, 1\}$, $S = 1$ represents successful assembly. The goal is to model probability $P(S = 1|x, y, z, V)$, which is subsequently written just as P.

The parameters first scaled into dimensionless form by

$$\tilde{x} = \frac{x}{s}, \qquad \tilde{y} = \frac{y}{s}, \qquad \tilde{z} = \frac{z}{s}, \qquad \tilde{d} = \frac{(12V/\pi)^{1/3}}{s} \tag{1}$$

where s is the lateral dimension of the part. The droplet volume is replaced by dimensionless diameter of the droplet by approximating the droplet with a half-sphere. More accurate approximations would only affect the scaling constant.

We use logistic regression [39] to model success rate as a function of the parameters. Logistic regression is a well-established method used for prediction of the probability of occurrence of an event as a function of explaining variables. The regression model is

$$P = \frac{1}{1 + e^{-w}} \tag{2}$$

where $w = \boldsymbol{\theta}^T \mathbf{X}$, with $\boldsymbol{\theta}$ being the coefficient vector $(M \times 1)$, and $\mathbf{X}$ being a vector $(M \times 1)$ that contains all the explaining variables, i.e.,

$$\mathbf{X} = [\,1 \quad \tilde{x} \quad \tilde{y} \quad \tilde{z} \quad \tilde{d} \quad \tilde{x}^2 \quad \tilde{x}\tilde{z} \quad \tilde{x}\tilde{d} \quad \tilde{y}^2 \quad \tilde{y}\tilde{z} \quad \cdots \quad \tilde{z}^2\,]^T. \tag{3}$$

The total number of explaining variables $M = 15$. The second-order terms are included in the model to account for symmetrical dependencies because the success rate is expected to drop when bias is either small or large.

The likelihood L of the model is defined as

$$L = \prod_{i=1}^{N} \left\{ P_i^{S_i} (1 - P_i)^{(1-S_i)} \right\} \tag{4}$$

where N is the total number of tests, P_i is the predicted probability of the ith test, and S_i is the outcome of the ith test. *Maximum likelihood estimate* of the model coefficients is found by numerically optimizing $\boldsymbol{\theta}_{\mathrm{ML}} = \mathrm{argmax}_{\boldsymbol{\theta}} L$.

The model can be used to predict the probability of successful assembly, given the parameters. Furthermore, the model can be used to find optimal parameters (x^*, y^*, z^*, V^*).

$$\begin{aligned} (x^*, y^*, z^*, V^*) &= \arg\max_{x,y,z,V} P, \qquad \text{subject to} \\ x &\in [x_{\min}, x_{\max}], \qquad y \in [y_{\min}, y_{\max}] \\ z &\in [z_{\min}, z_{\max}], \qquad V \in [V_{\min}, V_{\max}] \end{aligned} \tag{5}$$

i.e., the optimal values are sought only in the parameter range, which was tested. Finally, the model can be used to predict the optimal success rate P^*.

D. Model Validation

To validate our model, three different validation methods are used to avoid shortcomings of any one particular method.

1) G-Statistic: Deviance D [40] is a measure of the explaining power of the model

$$D = -2 \ln L. \tag{6}$$

To validate the model, we compare our *full* model, which includes all the explaining variables, with *intercept* model, which includes only the constant term. Model validation can be done using *G-statistic* [41], which is defined as

$$G = D_{\mathrm{Intercept}} - D_{\mathrm{Full}} \propto \chi^2_{p-2} \tag{7}$$

where $D_{\mathrm{Intercept}}$ is the deviance for the intercept model, D_{Full} is the deviance for the full model, and p is the number of parameters in the model. G-statistic follows chi-square (χ^2) distribution with $p - 2$ degrees of freedom, which can be used as a basis of validation. The threshold to accept the modeling is set at 5% level so that the criterion to accept the modeling is (the larger G-statistic the better) $P(\chi^2_{p-2} > G) < 0.05$.

2) Hosmer–Lemeshow Statistic: Another common validation statistic for logistic regression is *Hosmer–Lemeshow (HL)* statistic [39]. HL-statistic is calculated by dividing the data into ten bins according to their predicted probabilities. Then

$$\mathrm{HL} = \sum_{j=1}^{10} \frac{(O_j - E_j)^2}{E_j(1 - E_j/n_j)} \propto \chi^2_8 \tag{8}$$

where O_j is the observed number of successes in bin j, $E_j = \sum_{i \in \mathrm{bin}\,j} P_i$ is the expected number of success in bin j, and n_j is the number of tests in bin j. Fixed bin size is used, i.e., first bin contains all the tests with $0 \le P_i < 0.1$. HL-statistic follows a χ^2 distribution with 8 DOF. The threshold to accept the modeling is set at 5% level so that the criterion to accept the modeling is (the smaller the HL-statistic the better) $P(\chi^2_8 > \mathrm{HL}) > 0.05 \Leftrightarrow \mathrm{HL} < 15.5$.

3) Pseudo-R^2 Statistics: Finally, we quote pseudo-R^2 statistics [41] to measure the goodness-of-fit of our models. Pseudo-R^2 statistics take values that range from 0 to 1, higher values that denote better match between the predicted values and the outcome. We calculate McFadden's and Nagelkerke's pseudo-R^2 as follows:

$$R^2_{\text{McFadden}} = 1 - \frac{\ln L_{\text{Full}}}{\ln L_{\text{Intercept}}} \tag{9}$$

$$R^2_{\text{Nagelkerke}} = \frac{1 - \left\{\frac{L_{\text{Intercept}}}{L_{\text{Full}}}\right\}^{2/N}}{1 - L^{2/N}_{\text{Intercept}}} \tag{10}$$

where L_{Full} is the likelihood of the full model with all explaining variables, and $L_{\text{Intercept}}$ is the likelihood of the intercept model. McFadden's R^2 value tends to be smaller than the classical R^2 value, and values of 0.2 and 0.4 are considered highly satisfactory [42]. However, there has been an argument if pseudo-R^2 values are really good for anything else than to compare two models of the same data [43]; therefore, readers are cautioned not to base their judgment solely on the pseudo-R^2 values, but they should also consider the G-statistic and HL-statistic.

E. Elimination of Explaining Variables

To reduce unnecessary model complexity, the model is simplified by stepwise elimination of the explaining variables. In the initial model, all 15 variables are included. At each step, the variable whose removal from the model increases the deviance the least is eliminated. To test whether a variable is significant, G-statistic difference between the model with and without the variable is calculated

$$\Delta G = G_1 - G_0 \propto \chi^2_1 \tag{11}$$

where G_1 is the G-statistic for the model without the variable, and G_0 is the G-statistic for the model with the variable. The elimination is stopped when $P(\chi^2_1 > \Delta G) < 0.005$, i.e., when the model with the variable has larger than 0.5% chance of being better (as measured by deviance) than the model without the variable.

F. Results of Statistical Modeling

Using logistic regression and elimination of variables, the resulting models are

$$w_1 = -6.83 + 11.29\tilde{d} - 216.93\tilde{z}^2 + 79.80\tilde{z}\tilde{d} \tag{12}$$

$$w_2 = -15.36 + 63.28\tilde{d} - 11.73\tilde{x}^2 - 10.20\tilde{y}^2 - 170.23\tilde{z}^2 + 83.94\tilde{z}\tilde{d} - 60.07\tilde{d}^2 \tag{13}$$

$$w_3 = 3.71 - 7.48\tilde{x}^2 - 9.31\tilde{y}^2 - 1.62\tilde{y}\tilde{d} - 61.23\tilde{z}^2 + 26.06\tilde{z}\tilde{d} - 2.82\tilde{d}^2 \tag{14}$$

where w_i is the regression model for test set i. Using (1) and (2), the models can be used to calculate yield P as a function of process parameters.

For all test sets, the optimal yield and corresponding droplet volume and z-bias can be calculated (see Table II). In test set 1, the optimal droplet volume predicted by the model was limited by the upper bound of the tested parameter range, i.e., even larger droplet volumes could have been tested to increase the success rate.

TABLE II
OPTIMAL PARAMETERS AND YIELD IN EACH TEST SET

	Test set 1	Test set 2	Test set 3
x^* (μm)	-	0	0
y^* (μm)	-	0	-11.9
z^* (μm)	40.0	47.1	29.3
V^* (nl)	2.7	1.8209	0.6800
P^*	99.47%	99.16%	97.71%

TABLE III
VALIDATION STATISTICS FOR REGRESSION MODELS

	Test set 1	Test set 2	Test set 3
G > threshold	102.9 > 6.0	244.3 >11.1	143.2 > 11.1
HL < threshold	10.3 < 15.5	4.5 < 15.5	5.9 < 15.5
R^2_{McFadden}	0.43	0.50	0.45
$R^2_{\text{Nagelkerke}}$	0.58	0.67	0.61

In (12), all explaining variables containing $\tilde{x}$ or $\tilde{y}$ were eliminated. Since P does not depend on $\tilde{x}$ or $\tilde{y}$ at all, optimal x^* or y^* could not be found.

In (13), the only terms that depend on $\tilde{x}$ or $\tilde{y}$ are the second-order terms, and their coefficients are negative; thus, the optimal $\tilde{x}$ or $\tilde{y}$ is found when the part is release exactly in the middle of the bottom part. In (14), there is a slight coupled dependence between $\tilde{y}$ and $\tilde{d}$, which results in optimal $y*$ at -11.9 μm.

In Table III, the validation statistics are quoted. For all modeling results, G-statistics are significantly larger than the corresponding thresholds, and HL statistics are significantly smaller than the corresponding thresholds, i.e., both have the desirable values. Furthermore, all pseudo-R^2 statistics are 0.58–0.67 (Nagelkerke) or 0.43–0.50 (McFadden). Thus, all validation statistics suggest good modeling results.

The results are further discussed in Section VI.

V. CAPABILITY, ACCURACY, AND SPEED

To further assess the hybrid assembly technique, we measure the capabilities, accuracy, and speed of the process. Capability is a qualitative measure of how well the assembly method can be adopted for various assembly tasks. This is assessed by testing parts of various sizes and shapes. Accuracy is a quantitative measure, which is measured in micrometers, of how well the assembled part is positioned to the desired location after completion of the assembly. This is measured by studying the final assembly results under an SEM. Speed is a measure of the time duration that takes to complete the assembly. With the assistance of a high-speed camera, the duration and trajectories of droplet self-alignment of the hybrid assembly process are studied.

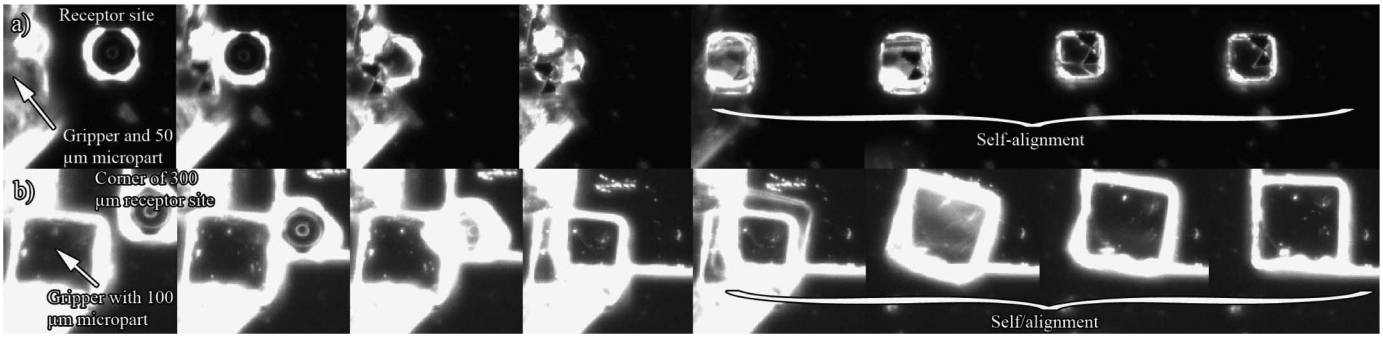

Fig. 10. Two different sequences show the capability of the hybrid handling method. Handling of (a) 50 × 50 × 40 μm^3 microparts and (b) 100 × 100 × 70 μm^3 micropart to the corner of a bigger part, where the gripper approaches with a part from the left in both cases.

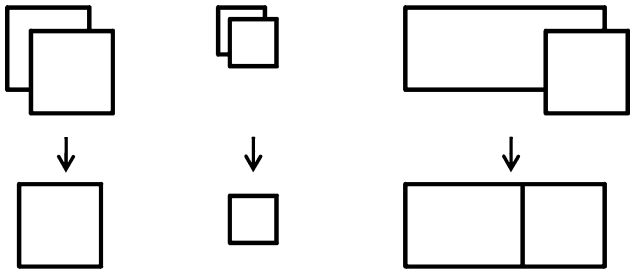

Fig. 11. Assembly cases for measuring accuracy.

A. Capability

In addition to the largely proven 300 μm × 300 μm × 70 μm parts, hybrid assembly of 50 μm × 50 μm × 40 μm [see Fig. 10(a)] on top of receptor sites with equal size was tested. The parameters were varied from test to test within a reasonable range. Out of 20 tests, 16 were successful.

Moreover, assembly of different-sized parts was studied, where 100 μm × 100 μm × 70 μm sized parts are assembled on top of much larger parts. The theoretic concept of assembly different-sized parts has been discussed in Section II-D. Here, we experimentally verify this concept by starting the self-alignment outside a corner. This will fix all DOF [see Fig. 10(b)]. The experiment was repeated 39 times, with different initial bias and number of droplets. Out of these tests, 37 (95%) were successful.

B. Accuracy

To study the accuracy of the hybrid handling, final assembly results were inspected using an SEM. Three sets of tests were performed.

1) 300 μm × 300 μm × 40 μm on top of 300 μm × 300 μm × 40 μm parts;
2) 100 μm × 100 μm × 40 μm on top of 100 μm × 100 μm × 40 μm parts;
3) 300 μm × 300 μm × 40 μm parts in the end of 300 μm × 600 μm × 40 μm bars.

In case 3), the part will align to the end of the bar if the release position is started outside the bar, as discussed in Sections II-D and V-A. The assembly cases are illustrated in Fig. 11.

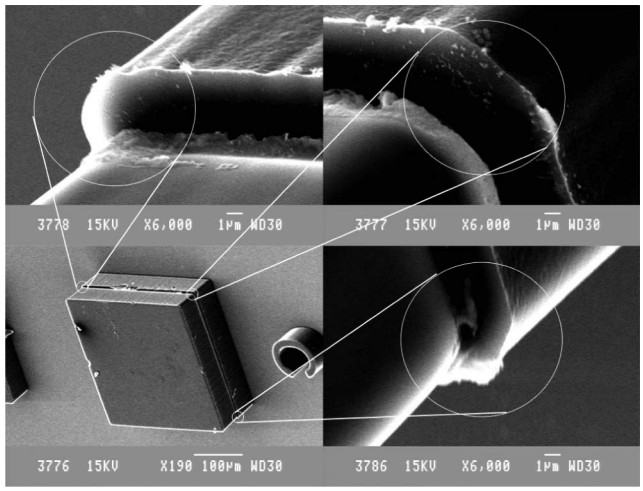

Fig. 12. Measuring the assembly accuracy by an SEM.

TABLE IV
ERROR FOR 300 × 300 PARTS

#	x-error (μm)	y-error (μm)	angle error (°)
1	-0.1	3.1	0.0
2	-0.5	3.3	-0.2
3	-2.6	-0.6	0.2
4	-2.6	1.7	0.0
5	-2.2	-0.8	-1.0
6	-0.6	-1.1	0.0
RMS	**1.8**	**2.0**	**0.4**
MA	**1.5**	**1.8**	**0.2**

Because of the manufacturing imperfections in the parts, the part and the receptor site did not exactly match in size. Therefore, the translational accuracy was measured by calculating the difference between the geometrical centers of the parts. The SEM images used for one such analysis are shown in Fig. 12. For assembly case 3), error measurements only in y-direction could be done so that only y-error and angle error are quoted. The results are given in Tables IV–VI, along with rms and mean-absolute values.

TABLE V
ERROR FOR 100 × 100 PARTS

#	x-error (μm)	y-error (μm)	angle error (°)
1	2.1	2.4	0.4
2	2.1	-0.6	-0.4
3	0.2	2.1	0.0
4	-2.1	0.1	-0.4
5	-2.4	-3.7	0.5
RMS	**1.9**	**2.2**	**0.4**
MA	**1.8**	**1.8**	**0.4**

TABLE VI
ERROR FOR 300 × 300 PARTS ON LARGER PARTS

#	y-error (μm)	angle error (°)
1	-2.7	-0.5
2	-0.8	0.6
3	-3.4	0.1
4	0.2	0.2
5	-1.8	0.0
6	0.4	0.2
7	-7.5	0.3
RMS	**3.4**	**0.3**
MA	**2.4**	**0.3**

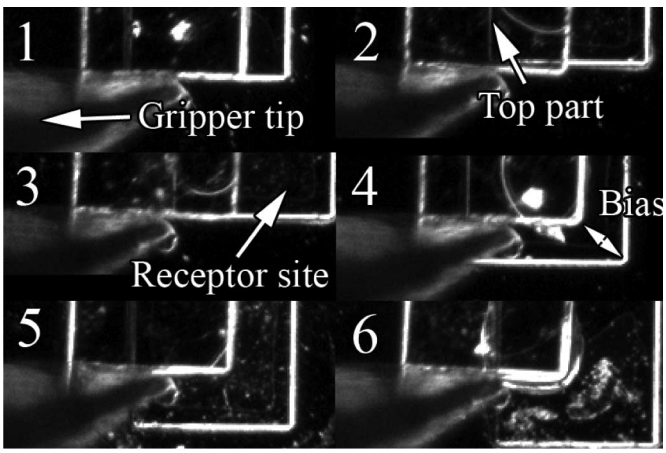

Fig. 13. Six different release positions.

C. Speed

Using the high-speed camera, we measured the duration of the self-alignment of the hybrid handling process for parts of the size 300 μm × 300 μm × 70 μm. Six test sets were done, each set with a different initial bias. The self-alignment time is measured by finding the frames from the high-speed video when the gripper opens and when there is no noticeable movement of the micropart. Three of the test sets have bias only in the x-direction, and three have bias in both the x- and y-direction. Different release positions are shown in Fig. 13. 1.2 nL of water was used in each test. Each test set has 15 repetitions, except that the test set 6 had only 12 repetitions. The results are summarized in Table VII.

There are rather large variations in the duration of the self-alignment, even if the releasing position is almost the same

TABLE VII
SELF-ALIGNMENT TIMES

#	x-bias (μm)	y-bias (μm)	Self-alignment duration (ms)	Standard deviation (ms)
1	-85	-2	27.0	4.6
2	-156	-19	72.5	16.2
3	-188	-8	274	146
4	-90	75	29.6	18.5
5	-123	105	56.8	29.3
6	-179	127	77.3	50.8

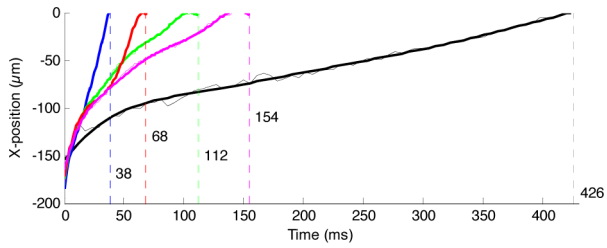

Fig. 14. X-position as a function of time of five tests from test set 3. There is an order-of-magnitude difference in the self-alignment time between the two extreme cases.

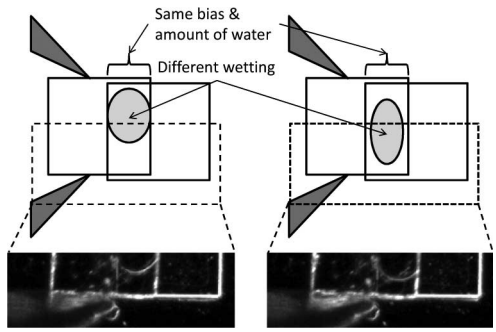

Fig. 15. Initial positions for two extreme cases of self-alignment from Fig 14. Notice that the positions are otherwise very similar, except for small differences in the initial wetting shape of the liquid. Only a small portion of the image was recorded due to the high-speed recording with reduced AOI.

in each test. To illustrate such large variations in self-alignment time and trajectories, five example trajectories are selected from the test set 3. The trajectories of the microparts are shown in Fig. 14. The starting positions are almost the same, except for the shape of the meniscus. The self-alignment is successful in all cases. However, the duration of the self-alignment varies significantly. In the two extreme cases, one took 426 ms and the second 38 ms. The difference in initial meniscus for these cases is shown in Fig. 15.

VI. DISCUSSION

A. Key Process Parameters

1) x- and y-Bias: In test set 1, there is no clear trend in the yield with respect to x- or y-bias, even when the bias approaches 250 μm. This can be seen in the regression model: All variables that depend on x- or y-bias were eliminated from the regression model.

In test sets 2 and 3, the optimal x-bias and y-bias were found when the top part was exactly in or very close to the middle

of the bottom part because the yield drops almost to zero when the bias moves the center of the part outside the receptor site, and the dispensing fails. In test set 3, the $\tilde{y}^2$ term is larger than the $\tilde{x}^2$ term, which may be because of the gripper tips that grab the chip in the y-direction, which results in some velocity in the y-direction when releasing. Also, in test set 3, the optimum was found when y-bias was slightly off-center; this may be because of the successful dispensing area not being exactly in the center of the bottom part and because of the tilt of the dispenser. Therefore, the model may be slightly unsymmetric.

In general, x- bias and y-bias were not very critical for the process: For instance, in test set 3, the yield drops to 98% only after the x-bias is outside ± 82 μm, and the y-bias is outside ± 88 μm if other parameters are kept optimal.

2) z-Bias and Droplet Volume: In test sets 2 and 3, coupling in the droplet volume and z-bias can be seen. This resulted in the inclusion of the cross term $\tilde{z}\tilde{d}$ in the regression model. The larger the number of droplets, the higher the z-bias that is needed for the successful assembly. This is because with a large amount of water and small z-bias, the water is squeezed between the part and the receptor site. The result is that the water spills over the sides of the parts, and the assembly typically fails. The optimal droplet volume in test set 2 is smaller than that in test set 1 because of the larger droplets easily overflowing when they are dispensed close to the border of the receptor site. In test set 1, larger droplets can be used as they are always exactly in the middle of the bottom part.

In test set 2, over 98% yield is achieved when z-bias is between 25 and 69 μm, or droplet volume is between 0.97 and 3.07 nL, if other parameters are kept optimal. Compared with the optimal x-bias and y-bias, the optimum is nontrivial. Therefore, it is concluded that for a successful hybrid microassembly, one should try to optimize the amount of water and z-bias to achieve good yield.

B. Extension of the Results to Other Part Sizes, Shapes, and Liquids

In test set 3, the optimal z-bias and droplet volume are smaller than that in test set 2. However, clearly, the optimal volume does not scale according to s^3 because the predicted optimal volume for data 3 based on data 2 would then be only 0.067 nL. Further testing should be carried out to experimentally find the yield as a function of scale, but for part sizes between or close to 100 μm $\times$ 100 μm $\times$ 40 μm and 300 μm $\times$ 300 μm $\times$ 70 μm, linear interpolation/extrapolation between the models 2 and 3 may offer a reasonable starting point as the models are very similar.

The basic yield trends as function of input parameters are expected to extend to various other liquids also; however, the maximum achievable success rates are expected to be liquid specific. Most important liquid properties that affect the self-alignment process are the wetting properties (e.g., contact angles) of the surfaces and the viscosity of the liquid. We have observed that highly wettable surfaces are beneficial to the water droplet self-alignment, which contribute positively to the yield. Viscous liquids may develop bubbles during wetting [44], which is expected to contribute negatively to the yield.

The droplet self-alignment only requires matching or closely matching surface shapes to work. The surface shapes should be designed so that there are no local minima between starting position and assembly position, and the force is always large. This requirement is more relaxed than in pure self-assembly. Otherwise, the 3-D shape of the receptor site and the micropart can be chosen quite freely. Therefore, while the assembled structures in this study were only rather 2.5-D structures, we have also shown that the assembly method can be used for different 3-D structures as well [45].

When scaling the size of the parts further down, the limiting factor is the minimum amount of water that could be dispensed using our setup. However, other suitable methods to deliver smaller amounts of liquid (e.g., contact printing) exist; thus, the results of this study should still be relevant, even for smaller parts than what was tested in this paper.

C. Comparison With Self-Assembly and Robotics

With optimal bias and droplet volume, high success rates (99.47%, 99.16%, and 97.71% for test sets 1–3, respectively) could be achieved. This is generally quite high as compared with the yields reported in fluidic self-assembly, which range from 62% to claimed 100% and 97% typical [46].

The accuracy tests show that assembly accuracies close to the fabrication accuracy of the mask, which are better than the fabrication accuracy of the microparts (approximately 2 μm), can be achieved. This kind of accuracy is comparable with the accuracy achieved by self-assembly methods, which range from claimed 0.3 μm [46] to 10 μm and 2 μm typical [47], which is not surprising since the accuracy of the method is fixed by the droplet self-alignment. Microparts with better definition should be used to find out what are the limits in accuracy of the method.

It can be argued that the proposed hybrid assembly has at least similar or even better accuracy than the best conventional robotics solutions. Moreover, to achieve precise assembly using robotic microhandling, a proper fixing strategy or bonding mechanism must be applied. Otherwise, the final assembly accuracy can be impaired by the adhesion of the part to the gripper during releasing.

In robotic microhandling, speed and accuracy are usually a tradeoff. Fast motion tends to be less accurate, and to achieve high accuracy, smooth and slow motions are needed to reduce dynamic errors, such as overshoot and oscillations.

Because of this, the robotic pick-and-place process and the self-alignment process are two relatively independent processes, and the hybrid microassembly robot can start assembling the next part before the previous self-alignment has finished. Therefore, hybrid microhandling can be carried out in the maximum cycle time of the robot despite the assembly period of the self-alignment process. As the previous tests have shown, much more inaccurate, and therefore faster, positioning systems can be used. For example, a modern industrial robot can place submillimeter parts at a throughput of tens of parts per second at a relatively low accuracy of 10 μm [19]. The self-alignment time

would then be comparable with the time of the pick-and-place operations. The benefit of the proposed approach is that the accuracy would not be greatly affected, even when using ultra high-speed and inaccurate robotics.

Whereas it was clear from the previous studies [48] that the self-alignment takes typically in the order of tens or hundreds of milliseconds, what is interesting is that there are rather large variations in the duration of the self-alignment, even if the releasing position is almost the same in each test. Small errors in position and tilting of the part and the amount and the position of the liquid, which combined with small imperfections of the part surfaces and friction, can lead to very different initial wetting. Thus, the dynamics can be very different from test to test. It is rather hard to explain the trajectories if perfect surfaces with perfect wetting are assumed.

VII. Conclusion

We have reported a study of a hybrid microassembly technique, which combine robotic microgripper with water droplet self-alignment, to position microparts to well-defined locations and orientations.

With suitable process parameters, yields of over 99% can be achieved. As long as the water droplet is dispensed on top of the receptor site and the assembled part touches the droplet and forms a meniscus, even inaccurate pick-and-place robot, which has a poor positioning accuracy (e.g., tens of micrometers) in the x-axis and the y-axis, can lead to reliable assembly. Using logistic regression, the yield of the assembly technique was shown to be mostly depended on the amount of water and z-bias used, especially when dispensing the water in the middle of the receptor site. The final assembly accuracy can be much better than the accuracy of the positioning systems. This potentially leads to huge cost savings in industrial assembly robotics. The basic results of this study should be extendable to different part sizes, different receptor site configurations, and even different liquids.

Moreover, self-alignment of parts of having different sizes has hardly been studied. This experimental study shows that parts of different sizes can be reliably assembled using such a hybrid method. This, combined with using only the solid edge to constrain the liquid, reduces requirements on the fabrication of the microparts and the receptor sites so that the design and fabrication of the parts and receptor sites are less coupled.

The duration of self-alignment process was measured to range from around 50 to 500 ms, which is reasonably fast for industrial applications. The random nature of the process leads to large variations in the duration of the self-alignment from one test to another. However, this does not affect the final results, as the parts will reliably go to the desired position, if the process parameters are well chosen.

References

[1] G. Campardo, G. Ripamonti, and R. Micheloni, "3-D integration technologies," *Proc. IEEE*, vol. 97, no. 1, pp. 5–8, Jan. 2009.

[2] G. Q. Zhang, M. Graef, and F. van Roosmalen, "Strategic research agenda of 'More than Moore,'" in *Proc. 7th Int. Conf. Therm., Mech. Multiphys. Simul. Exp. Micro-Electron. Micro-Syst.*, Milano, Italy, 2006, pp. 1–6.

[3] R. A. Russell, "A robotic system for performing sub-millimetre grasping and manipulation tasks," *Robot. Auton. Syst.*, vol. 13, pp. 209–218, 1994.

[4] U. Rembold and S. Fatikow, "Autonomous microrobots," *J. Intell. Robot. Syst.*, vol. 19, pp. 375–391, 1997.

[5] B. Vikramaditya and B. J. Nelson, "Visually servoed micropositioning for robotic micromanipulation," *J. Microcomput. Appl.*, vol. 18, no. 1, pp. 23–31, 1999.

[6] J. T. Feddema and R. W. Simon, "Visual servoing and CAD-driven microassembly," *IEEE Robot. Autom. Mag.*, vol. 5, no. 4, pp. 18–24, Dec. 1998.

[7] Q. Zhou, A. Albut, C. del Corral, P. J. Esteban, P. Kallio, B. Chang, and H. N. Koivo, "A microassembly station with controlled environment," in *Proc. SPIE Microrobot. Microassembly III*, Boston, MA, 2001, vol. 4568, pp. 252–260.

[8] N. Dechev, W. L. Cleghorn, and J. K. Mills, "Microassembly of 3-D microstructures using a compliant, passive microgripper," *J. Microelectromech. Syst.*, vol. 13, no. 2, pp. 176–189, 2004.

[9] A. Ferreira, C. Cassier, and S. Hirai, "Automatic microassembly system assisted by vision servoing and virtual reality," *IEEE/ASME Trans. Mechatron.*, vol. 9, no. 2, pp. 321–333, Jun. 2004.

[10] J. N. Israelachvili, D. J. Mitchell, and B. W. Ninham, "Theory of self-assembly of hydrocarbon amphiphiles into micelles and bilayers," *J. Chem. Soc., Faraday Trans.*, vol. 2, pp. 341–365, 1976.

[11] R. N. Perham, "Self-assembly of biological macromolecules," *Philos. Trans. Roy. Soc. London B*, vol. 272, no. 915, pp. 123–136, 1975.

[12] M. B. Cohn, C. J. Kim, and A. P. Pisano, "Self-assembling electrical networks: An application of micromachining technology," in *Proc. 6th Int. Conf. Solid-State Sens. Actuators*, 1991, pp. 490–493.

[13] H.-J. J. Yeh and J. S. Smith, "Fluidic self-assembly for the integration of GaAs light-emitting diodes on Si substrates," *IEEE Photon. Technol. Lett.*, vol. 6, no. 6, pp. 706–708, Jun. 1994.

[14] K. F. Böhringer, K. Goldberg, M. Cohn, R. Howe, and A. Pisano, "Parallel microassembly with electrostatic force fields," in *Proc. IEEE Int. Conf. Robot. Autom.*, 1997, pp. 1204–1211.

[15] U. Srinivasan, D. Liepmann, and R. T. Howe, "Microstructure to substrate self-assembly using capillary forces," *J. Microelectromech. Syst.*, vol. 10, pp. 17–24, 2001.

[16] X. Xiong, Y. Hanein, J. Fang, Y. Wang, W. Wang, D. T. Schwartz, and K. F. Böhringer, "Controlled multi-batch self-assembly of micro devices," *ASME/IEEE J. Microelectromech. Syst.*, vol. 12, no. 2, pp. 117–127, Apr. 2003.

[17] G. M. Whitesides and B. Grzybowski, "Self-assembly at all scales," *Science*, vol. 295, pp. 2418–2421, 2002.

[18] S. Kim, E. Saeedi, J. Etzkorn, and B. A. Parviz, "Large scale self-assembly of crystalline semiconductor microcomponents onto plastic substrates via microfluidic traps," in *Proc. 4th Annu. IEEE Conf. Autom. Sci. Eng.*, Washington, DC, 2008, pp. 967–970.

[19] Assémbleon. Pick & Place equipment. (2009). [Online]. Available: http://www.assembleon.com/surface-mount-assembly/pick-and-place-equipment/

[20] Alien Technol., FSA technology. (2010). [Online]. Available: http://www.alientechnology.com/fsa_manufacturing.php

[21] H. Aoyama, F. Iwata, J. Fukaya, and A. Sasaki, "Miniature robot with micro capillary probe for surface clearing operation," *J. Robot. Mechatron.*, vol. 7, no. 6, pp. 488–492, 1995.

[22] A. Ashkin, J. M. Dziedzic, J. E. Bjorkholm, and S. Chu, "Observation of a single-beam gradient force optical trap for dielectric particles," *Opt. Lett.*, vol. 11, pp. 288–290, 1986.

[23] S. Haliyo, S. Régnier, and Ph. Bidaud, "Manipulation of micro-objects using adhesion forces and dynamical effects," *Exp. Robot. VIII*, vol. 5, pp. 382–391, 2003.

[24] J. Fang and K. F. Böhringer, "Parallel micro component-to-substrate assembly with controlled poses and high surface coverage," *IOP J. Micromech. Microeng.*, vol. 16, pp. 721–730, 2006.

[25] V. Sariola, Q. Zhou, and H. N. Koivo, "Hybrid microhandling: A unified view of robotic handling and self-assembly," *J. Micro-Nano Mechatron.*, vol. 4, no. 1, pp. 5–16, 2008.

[26] Q. Zhou and V. Sariola, "Unified view of robotic microhandling and self-assembly," in *Robotic Microassembly*, M. Gauthier and S. Régnier, Eds. Piscataway, NJ: IEEE Press, 2010, pp. 109–144.

[27] Q. Zhou and B. Chang, "Microhandling using robotic manipulation and capillary self-alignment," in *Proc. IEEE/RSJ Int. Conf. Intell. Robots Syst.*, 2006, pp. 5883–5888.

[28] H. Tsunetsugu, T. Hayashi, K. Katsura, M. Hosoya, N. Sato, and N. Kukutsu, "Accurate, stable, high-speed interconnections using 20- to 30-μm-diameter microsolder bumps," *IEEE Trans. Compon. Packag. Manuf. Technol. Part A:*, vol. 20, no. 1, pp. 76–82, Mar. 1997.

[29] K. Moon, J. Wu, and C. P. Wong, "Study on self-alignment capability of electrically conductive adhesives (ECAs) for flip-chip application," in *Proc. Int. Symp. Adv. Packag. Mater.: Process., Properties Interfaces*, 2001, pp. 341–346.
[30] K. Sato, K. Ito, S. Hata, and A. Shimokohbe, "Self-alignment of microparts using liquid surface tension—behavior of micropart and alignment characteristics," *Precision Eng.*, vol. 27, no. 1, pp. 42–50, 2003.
[31] C. G. Tsai, C. M. Hsieh, and J. A. Yeh, "Self-alignment of microchips using surface tension and solid edge," *Sens. Actuators, A*, vol. 139, no. 1–2, pp. 343–349, 2007.
[32] C. del Corral, Q. Zhou, A. Albut, B. Chang, S. Franssila, S. Tuomikoski, and H. N. Koivo, "Droplet based self-assembly of SU-8 microparts," in *Proc. 2nd VDE World Microtechnol. Congr.*, Munich, Germany, 2003, pp. 293–298.
[33] M. Kaneda, M. Yamamoto, K. Nakaso, T. Yamamoto, and J. Fukai, "Oscillation of a tilted circular pad on a droplet for the self-alignment process," *Precision Eng.*, vol. 31, no. 2, pp. 177–184, 2007.
[34] P. Lambert and S. Régnier, "Surface and contact forces models within the framework of microassembly," *J. Micromechatron.*, vol. 3, no. 2, pp. 123–157, 2006.
[35] J. Lienemann, A. Greiner, J. G. Korvink, X. Xiong, Y. Hanein, and K. F. Böhringer, "Modelling, simulation and experimentation of a promising new packaging technology—Parallel fluidic self-assembly of micro devices," *Sens. Update*, vol. 13, no. 1, pp. 3–43, 2003.
[36] V. Sariola, Q. Zhou, R. Laaß, and H. N. Koivo, "Experimental study on droplet based hybrid microhandling using high speed camera," in *Proc. IEEE/RSJ Int. Conf. Intell. Robots Syst.*, Nice, France, 2008, pp. 919–924.
[37] A. Albut, Q. Zhou, C. del Corral, and H. N. Koivo, "Development of flexible force-controlled piezo-bimorph microgripping system," in *Proc. 2nd VDE World Microtechnol. Congr.*, Munich, Germany, 2003, pp. 507–512.
[38] S. Tuomikoski, C. del Corral, Q. Zhou, and S. Franssila, "SU-8 as a mechanical material: Gripper tips and microparts for a microassembly robot," presented at the 14th Micromechanic Workshop, Delft, The Netherlands, 2003.
[39] D. W. Hosmer and S. Lemeshow, *Applied Logistic Regression*, 2nd ed. New York: Wiley, 2000.
[40] D. W. Hosmer, S. Taber, and S. Lemeshow, "The importance of assessing the fit of logistic regression models: a case study," *Amer. J. Public Health*, vol. 81, no. 12, pp. 1630–1635, 1991.
[41] S. Menard, *Applied Logistic Regression Analysis*, 2nd ed. Newbury Park, CA: Sage, 2002.
[42] D. Tektas and S. Günay, "A Bayesian approach to parameter estimation in binary logit and probit models," *Hacettepe J. Math. Statist.*, vol. 37, no. 2, pp. 167–176, 2008.
[43] G. Hoetker, "The use of logit and probit models in strategic management research: Critical issues," *Strat. Mgmt. J.*, vol. 28, pp. 331–343, 2007.
[44] L. Yang, C. K. King, and J. B. Bernstein, "Liquid dispensing encapsulation in semiconductor packaging," *Microelectron. Int.*, vol. 20, no. 3, pp. 29–35, 2003.
[45] V. Sariola, Q. Zhou, and H. N. Koivo, "Three dimensional hybrid microassembly combining robotic microhandling and self-assembly," in *Proc. IEEE Int. Conf. Robot. Autom.*, 2009, pp. 2605–2610.
[46] Hoof, M. Mastrangeli, S. Abbasi, C. Varel, C. Van, J-P. Celis, and K. F. Böhringer, "Self-assembly from milli- to nanoscales: Methods and applications," *IOP J. Micromech. Microeng.*, vol. 19, pp. 83001–83037, 2009.
[47] B. P. Singh, K. Onozawa, K. Yamanaka, T. Tojo, and D. Ueda, "Novel high precision optoelectronic device fabrication technique using guided fluidic assembly," *Opt. Rev.*, vol. 12, no. 4, pp. 345–351, 2005.
[48] S.-H. Liang, X. Xiong, and K. F. Böhringer, "Towards optimal designs for self-alignment in surface tension driven micro-assembly," in *Proc. IEEE Conf. Micro Electro Mech. Syst.*, 2004, pp. 9–12.

Veikko Sariola received the M.Sc. degree in automation and systems technology from Helsinki University of Technology, Esbo, Finland, in 2007, where he is currently working toward the Ph.D. degree.

He is also currently with the Department of Automation and Systems Technology, School of Science and Technology, Aalto University, Aalto, Finland. His research interests include micro- and nanorobotic assembly, self-assembly of microscopic components, and hybrid microassembly.

Mirva Jääskeläinen received the M.Sc. degree in automation and system technology from Helsinki University of Technology, Esbo, Finland, in 2009.

She is currently with the Department of Automation and Systems Technology, School of Science and Technology, Aalto University, Aalto, Finland. Her research interests include the environmental effects on micro- and nanorobotic assembly and industrial applications of hybrid microassembly.

Quan Zhou (M'02) received the M.Sc. degree in control engineering and the Dr. Tech. degree in automation technology, both from Tampere University of Technology, Tampere, Finland.

Since 1995, he has been a Researcher or a Research Leader in Finland and China in nearly 20 academic, industrial, and European Union projects on micro- and nanorobotics and micromechatronics. He is the author or coauthor of more than 50 scientific publications. He is currently an Adjunct Professor with the Department of Automation and Systems Technology, School of Science and Technology, Aalto University, Aalto, Finland, where he is leading the Micro- and Nanorobotics Research Team. He was a Professor with the School of Mechatronics, Northwest Polytechnical University, Xi'an, China. His research interests include hybrid micro- and nanohandling, especially methods combining robotic manipulation and self-assembly, micro- and nanorobotics and automation, biomedical and surgical robotics, mobile microrobots, and artificial intelligence.

Prof. Zhou is currently the Coordinator of the EU-FP7 Project FAB2ASM.